Physiological Motion Compensation in Patch Clamping using Electrical Bio-impedance Sensing

Kaat Van Assche*, Yao Zhang*, Mouloud Ourak, Eric Verschooten,
Philip X. Joris, and Emmanuel Vander Poorten

***Abstract*— Patch clamping of neurons is a powerful technique used to understand the electrophysiological signals of the brain and advance research into neurological disorders. In in vivo patch clamping, a micropipette is clamped onto the membrane of a neuronal cell body. This technique is difficult and time-consuming to perform due to the challenges in approaching neurons because of their small size, the absence of visual feedback, and physiologically induced movement caused by heartbeat and breathing. This paper presents a model-based motion compensation algorithm relying solely on electrical bio-impedance (EBI) sensing. The ultimate goal is to cancel out the relative motion between the patch-pipette and the neuron to increase in vivo patch clamping efficiency. In the proposed algorithm, EBI-pipette measurements in response to physiologically induced motions are used to impose on the pipette a motion similar to that of the neuron. The model is based on the assumption that physiological motion can be approximated by a sinusoidal model with three parameters: frequency, phase, and amplitude. The developed compensation algorithm was evaluated in an experimental setup and results yielded a compensation efficiency of (85.5 ± 3.6)%, (81.9 ± 4.0)%, (75.9 ± 1.8)% for artificially imposed motions of 1 Hz, 2 Hz and 3 Hz with an amplitude of 31 µm. The algorithm also demonstrated that it can adjust its motion characterization in real time to changes in amplitude, phase, and also frequency.**

I. INTRODUCTION

Neurological disorders, such as Alzheimer's disease, Parkinson's disease [1] and hearing loss [2], are the second largest cause of death and the leading cause of disability in today's aging society [3]. However, even though they are increasingly prevalent, their underlying neurological mechanisms are still largely unknown. The brain is filled with billions of interconnected neurons, which together process a vast amount of information. To better understand the functioning of the brain, it is essential for scientists to be able to accurately measure in vivo the electrophysiological activity flowing through these neurons [4].

Patch clamping of neurons is one technique used to measure these signals. In this technique, a glass micropipette is moved towards the cell body of a neuron. Once it is close enough, slight suction is applied through the pipette. This results in the neuronal membrane being pulled tightly against the tip of the micropipette and creates a mechanical and electrical patch between the two. After this point, either extracellular or intracellular recordings can be made [5]. Traditionally, this technique is performed manually by the researcher. However, considering the micro-size of the neurons in a cerebral cortex, the lack of visibility makes this technique difficult and time consuming to perform. The researcher relies solely on voltage-time graphs to estimate when the pipette is in contact with the neuron and verify successful patch clamping [6]. Therefore, fully automated patch clamping systems are gaining in popularity and could provide a solution to optimizing the efficiency of the patch clamping process.

A major challenge in this procedure is the movement of the neurons caused by both heartbeat and breathing of the animal [7]. When the glass pipette electrode remains stationary at a certain distance from the neuron, these periodic physiological movements can cause the pipette to unintentionally penetrate the neuron. This movement adds additional complexity to the patch clamping technique as it prevents careful approach of the pipette toward the neuron and makes it harder to achieve a patch. This could damage the neuron and render it unusable, which requires the procedure to be restarted with a new pipette. Therefore, this paper presents a compensation algorithm that reduces the negative impact created by this physiologically induced motion and increases the efficiency of the patch clamping process.

The test animals used for patch clamping are often small rodents such as gerbils or chinchillas. The heart rate of gerbils and chinchillas under anesthesia is estimated to fall within a frequency range of 1 Hz to 3 Hz, based on rodent heart rates in literature [8], [9]. Therefore, the proposed compensation algorithm is designed to work and be validated within this frequency range.

To compensate for the induced motion generated by heartbeat and breathing, a linear finite impulse response (FIR) filter is proposed in [10] by filtering the electrocardiogram (ECG) and the respiratory pressure. A similar approach based on impulse response is also used for motion compensation in [11]. However, both of these two approaches require two different signals to characterize the physiological motion. This makes the whole system more complex and expensive. Besides relying on the physiological signal, visual feedback for in vivo stabilization is used in [12] with a high-speed camera. Advanced platforms proposed in [13], [14] provide the possibility for physiological motion compensation, which, however, still require skilled hands to operate. Besides

*These authors contributed equally to this work

K. Van Assche, Y. Zhang, M. Ourak, and E. Vander Poorten are with the Department of Mechanical Engineering, KU Leuven, Belgium (Corresponding author: Yao Zhang, Email: yao.zhang@kuleuven.be)

E. Verschooten and P. X. Joris are with the Laboratory of Auditory Neurophysiology, Leuven, Belgium

This project has received funding from an internal KU Leuven C3 project 3E200471 and a grant from the Belgian FWO [SB/1S96922N].

patch clamping in neuroscience research, different strategies in other medical applications for motion compensation are adopted. Examples include ultrasound imaging-assisted techniques for heartbeat motion [15], an electromagnetic sensor [16] and MRI-imaging protocol [17] for respiratory motion and machine/deep learning methods for registration-based motion during repositioning [18].

Differentiating from previous motion compensation, this paper presents a model-based compensation program that relies solely on Electrical Bio-impedance (EBI) measurements. EBI obtains the impedance by using a flow of electric current in a given circuit and hence eliminates the need for complex visioning systems [19], [20]. It is used increasingly in medical applications due to its low cost, high bandwidth, compact size, and good resolution [21], [22]. However, no exact impedance-distance relationship could be derived as the EBI recordings were found to be highly sensitive to the variations in physiological factors such as the conductivity of the medium. This leads to large differences in impedance-distance relationships between trials. In this study, we propose a compensation algorithm based on the characterization of phase, frequency, and amplitude of the relative changes in impedance. To the best of our knowledge, this paper is the first to present an impedance-distance relationship during the close approach of a pipette tip toward a tissue surface and the first paper to solely use impedance sensing in a closed-loop control as a means to compensate for the physiological motion in patch clamping.

The layout of this work is as follows. Section II discusses the observed variability in the impedance-distance relationship between the pipette tip and a target tissue. Section III explains the proposed model-based algorithm for ensuring physiological motion compensation. The next section IV presents the validation of this algorithm, including the experimental setup and the corresponding experimental results. Section V critically evaluates the feasibility of this model-based approach. Finally, section VI concludes the work and provides suggestions for future work.

II. Variability in Impedance-Distance Relationship

Initial experiments were performed to understand the impedance-distance relationship between a pipette electrode and cell tissue. Fig. 1 shows various impedance trials as a function of distance from the surface of a calf brain submerged in saline solution. Across trials, the results show significant variation in the relationship, but with a similar trend. At far distances, the impedance is constant and determined by the saline solution. Once the pipette approaches the surface of the tissue ($\sim$ 1 - 2 mm), the impedance increases rapidly (exponential-like) over a certain distance ($\sim$ 0.5 mm), after which it appears to slowly transition into a saturation region. The differences observed in this relationship across trials is because there is significant variability in factors such as the local concentration of the saline solution used to submerge the electrodes and the cell tissue. A change in saline concentration and hence medium conductivity highly affects

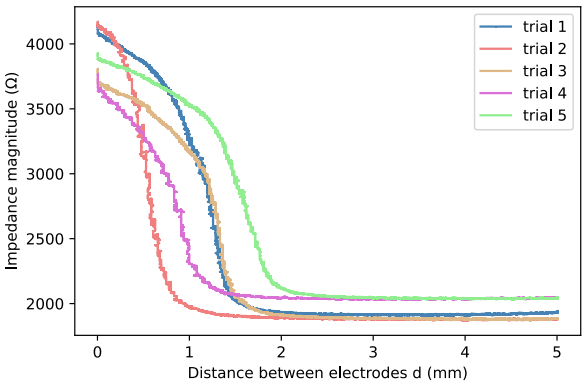


Fig. 1. Impedance-distance relationship of 5 consecutive trials when approaching a calf brain surface at 349 kHz with a 0.04s moving average window.

the impedance and challenges the reproducibility of the experiments. Furthermore, as two electrodes are submerged into the saline solution, an electrochemical reaction occurs at both electrode tips and the electrodes polarize, causing the sodium and chlorine ions to segregate. This further affects the local concentration of the saline solution and hence the impedance measurement [23]. This variability is already observed in the fairly well-controlled laboratory setup and will appear even more significantly in in vivo experiments. Obtaining a single impedance-distance relationship would motivate the use of feed forward control. However, due to this variability in impedance, we propose to determine a control signal based on relative changes in the impedance signal. Due to the inverse relationship, an increase in impedance corresponds to a decrease in the distance between the pipette tip and the neuron membrane and vice versa. This model forms the basis of the algorithm and feedback control could then be used to stabilize the entire system and cope with variability (such as noise) in the impedance sensor.

III. Physiological Motion Compensation Method

A. Overview of Compensation Algorithm

This paper presents a compensation method in which the effect of physiologically induced motion on neural tissue is compensated for by imposing a similar motion on the pipette, such that the relative motion is canceled. In this method, the pipette, in combination with EBI, is used as a sensor to measure a representation of the relative motion. For the intended application, the induced motion can be approximated by a sinusoidal waveform. In our approach, we take advantage of this and use a sinusoidal model in the compensation method where the frequency, phase, and amplitude are determined from the output signal of the sensor.

An important assumption made in this algorithm is that the physiological motion can be approximated by a sinusoidal waveform. Loschak *et al.* and Wood *et al.* indicated that both the respiratory and heartbeat motion have a near

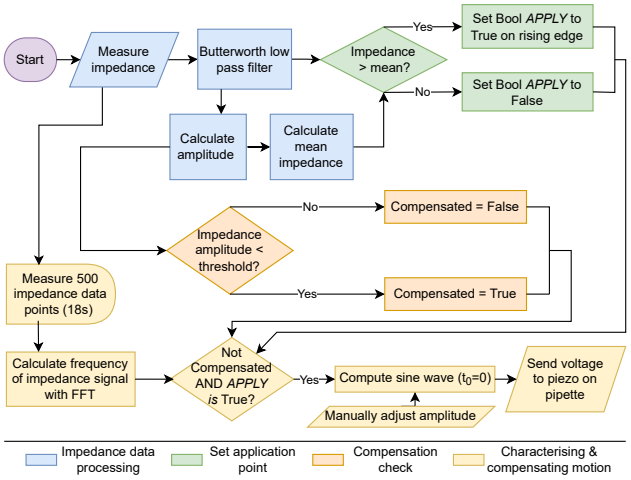


Fig. 2. Flowchart simplified compensation algorithm.

sinusoidal waveform [24], [25]. The superposition of both displacements would lead to a complex waveform with two sinusoidal components. Here, we assume that the heartbeat is dominant and that compensating for a single harmonic is sufficient. In the compensation algorithm, the heart rate-induced motion is assumed to be small and is approximated by a linear function. Therefore, the physiological motion and the EBI signal are expected to be similar. Both fundamental frequencies are always the same and their phases are locked in time, even with a $1/x$ relation. The main steps of this algorithm, written in LabVIEW®, are presented in the flowchart in Fig. 2.

B. Characterization Procedure

The first part of the characterization process of the algorithm focuses on determining the frequency of the physiological motion. A Fast Fourier Transform (FFT) module first calculates the frequency spectrum of the impedance signal and the algorithm then identifies its largest frequency component. The FFT module has a variable window, which can be determined by the user before the start of the program. The default window used for this paper is 500 data points. For a sample rate of 100 Hz, this leads to a first estimate after 5 seconds. After the first frequency is calculated, the algorithm continuously calculates and updates the frequency of the physiological motion. This relatively large window was chosen in order to maximize the accuracy and precision of the frequency calculation. For a small frequency error, the eventual phase shift between the two motions will be smaller and hence the compensation will be maintained longer. The disadvantage of using such a large window size is that the reaction speed is slower and hence a change in frequency will be detected with some delay. This trade-off must be carefully considered as a slow reaction speed could also prevent fast compensation and hence increase the chance of penetrating the neuron membrane. The first parameter, the frequency, of the sinusoidal physiological motion is now determined, which defines the frequency of the real-time compensation signal.

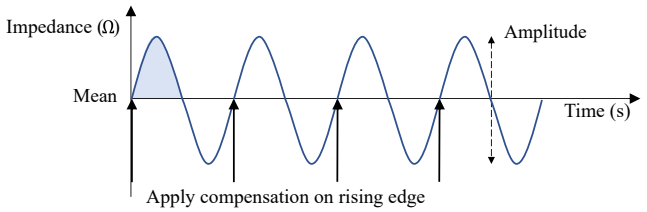


Fig. 3. Illustration of the impedance-time graph: the arrows show the zero phase point of the impedance signal, which corresponds to the point at which the compensating motion is applied.

The second parameter to characterize is the phase of the physiological motion to align the physiological motion and the compensation motion. This phase alignment is done by applying the compensation motion, with zero phase, at the moment the phase of the impedance signal is also equal to zero (aligning the zero-crossings at the rising slope). This application point is determined using the Boolean variable called APPLY. This zero phase point of the impedance signal is indicated by the solid arrows in Fig. 3 and is determined as follows. Both the mean and the peak amplitude of the impedance signal are continuously calculated. The mean impedance is determined by taking the average of the minima and maxima of the previous period. The positive half cycle, indicated by the blue shaded area, represents the points at which the real-time impedance is greater than the mean, and the exact transition point is determined at the rising edge. Exactly at the zero-crossing at the rising edge, the Boolean variable APPLY is set to True every two periods. Each time this APPLY variable is True and the physiological motion has not been compensated for (determined using a Boolean variable called COMPENSATED), the phase of the control signal will be reset to align with the impedance waveform. The compensation signal is reset by changing the time variable of the sine wave back to zero. This phase alignment procedure is repeated every two periods to ensure that the pipette stays in phase with the physiological motion throughout the patch clamping experiment. Therefore both the frequency and the phase can be updated regularly and hence conceptually, the motion will be compensated for, even with changes in frequency and phase. The amplitude is the last parameter required to fully determine the compensation signal. This parameter is adjusted manually by the user until the impedance amplitude is minimized and hence the compensated motion percentage is maximized.

C. Method to Determine Compensation

The following method is used as a criterion to indicate whether the motion is being compensated. Before any compensation signal is applied, the average amplitude of the EBI signal (A_0) is stored. Then, during compensation, when the EBI amplitude of the previous period (A_{k-1}) falls below a user-chosen threshold, such as e.g. 60% of (A_0), the program will signal that the motion is compensated using the Boolean variable called COMPENSATED. This EBI

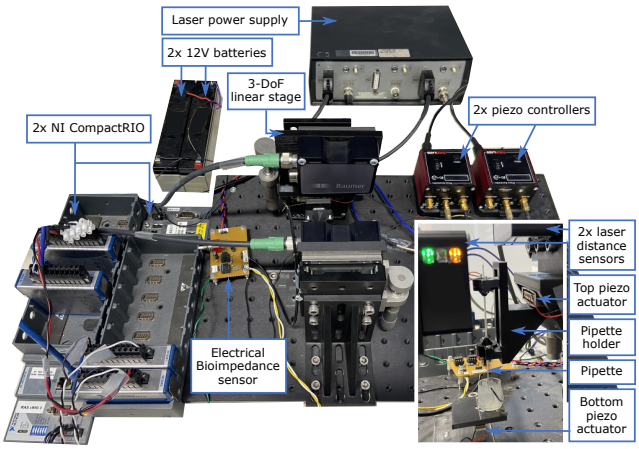


Fig. 4. Experimental setup: the bottom piezoelectric actuator simulates the physiological motion transferred to the plastic container, the top piezoelectric actuator realizes the compensation motion in the pipette. The distance moved by the pipette and the container is measured by a laser each and an EBI circuit is used to measure and characterize the physiological motion.

percentage threshold at period k is determined as follows:

$$\text{EBI compensation threshold}_k = \left(1 - \frac{A_{k-1}}{A_0}\right) \times 100. \quad (1)$$

The algorithm will stop updating the frequency and the phase of the compensated motion until the threshold is surpassed again. This will ensure that only the effect of an increase in compensation amplitude will be observed on the impedance-time graph and the compensation percentage. Therefore, smaller incremental changes in the amplitude of the compensation signal will be more visible and hence the optimal amplitude can be determined. If the phase and frequency change significantly during this manual adjustment step, the compensation percentage will fall below 60% again and these parameters can be corrected and updated again.

IV. Validation

A. Experimental Setup

In order to validate the compensation algorithm, an experimental setup was developed (Fig. 4). The EBI used in this study is custom-made and consists of a voltage-controlled current source and a special Field-Programmable Gate Array (FPGA) circuit (compacRIO, NI®) that generates the stimulus and performs instantaneous impedance calculations. The frequency at which the impedance is calculated is 156.25 Hz for a current of 0.1 µA, which is adequate for cell-based applications [26]. The impedance is measured between two electrodes. The positive electrode is connected to a glass pipette electrode (diameter 1.2 mm; filled with saline), and the negative electrode to a bath of saline (plastic container; 0.9 % solution) with a sheet of Parafilm® at the bottom to simulate the surface of a neuron.

The glass pipette is fixed in a pipette holder that is connected to a piezoelectric actuator (APF503, Thorlabs®, 310 µm stroke) [27], which is mounted to a 3-DoF linear stage. The piezoelectric actuator is the actual motion compensator and the linear stage is used to position and advance the pipette. In the experimental setup, an additional identical piezoelectric actuator is present to simulate the physiological motion. This actuator is connected to the bottom of the plastic container. Both actuators are controlled by a Kinesis piezo controller (KPZ101, Thorlabs®), allowing an operational bandwidth of 1 kHz. For validation, two laser sensors (OM70-11216505, Baumer® Group, Switzerland) were utilized to measure the motion of each actuator.

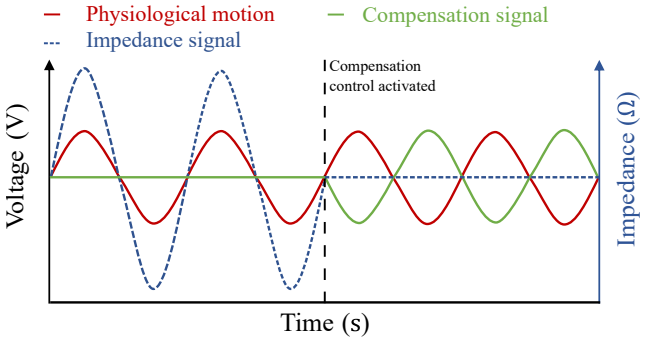


Fig. 5. Schematic representing the counterphase motion between the two piezoelectric actuators in relation to the impedance signal.

B. Phase Difference between Signals

It is important to note that the actuators for compensation and motion simulation are mounted in opposite directions and thus require opposite input polarities. However, because the EBI signal has an inverse relationship with distance (Fig. 1), the polarity of the compensation signal is opposite to that of the induced motion (Fig. 5). However, to simplify the visualization of both piezoelectric voltage signals, the controller signal is represented with a 180° phase shift in Fig. 6 and Fig. 7.

C. Results: Compensation Error

Two main experiments were performed to validate the efficacy of this compensation program. The first experiment quantified the compensation error, while the second experiment verified the reaction speed of the algorithm. The first experiment focused purely on compensating the simulated physiological motion with one fixed frequency, phase, and amplitude. Once the motion was induced, the compensation algorithm started to characterize the motion. In this step, the user blindly adjusted the amplitude of the compensation signal up to the point at which the EBI amplitude peaks were considered minimal. This was repeated five times for a set of frequencies (1 Hz, 2 Hz, 3 Hz). The result of one such trial at 2 Hz is shown in Fig. 6. These results show that the amplitude of the impedance signal gradually decreased with increasing compensating pipette motion until a chosen amplitude at which the motion was considered to be compensated.

The motion error was calculated by taking the difference between the physiological motion, i.e. the ground truth, and the controlled pipette motion measured by the two laser sensors during the last five periods. Four metrics were used to evaluate this error and the overview of the corresponding

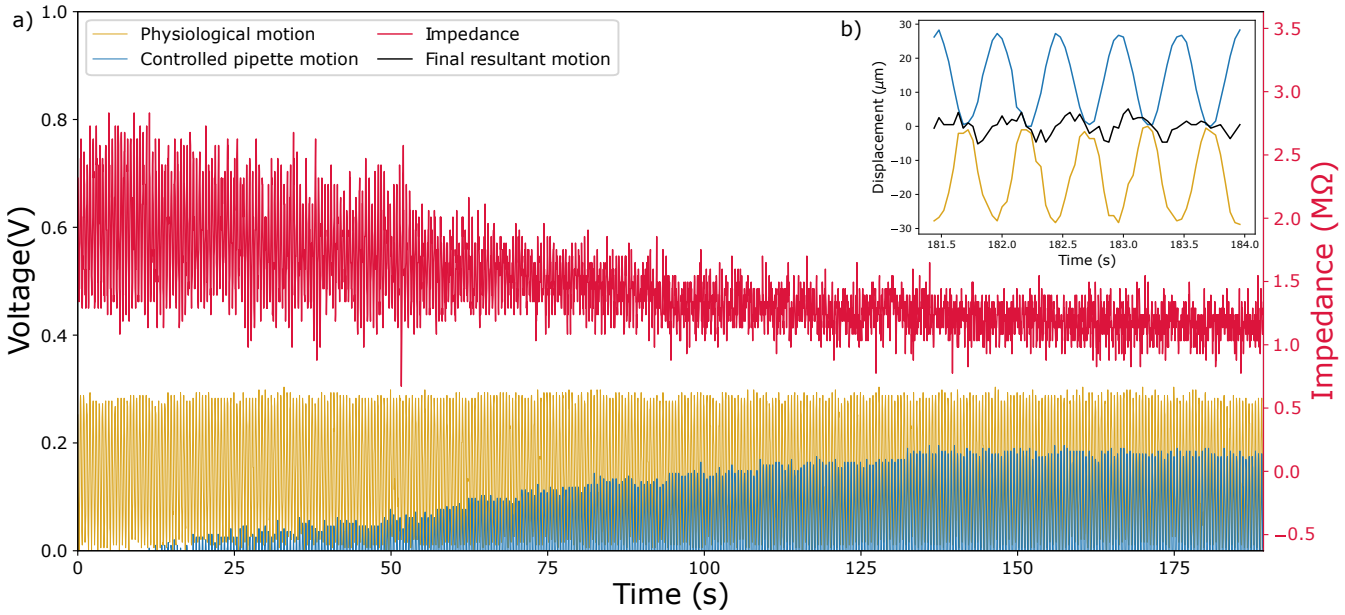


Fig. 6. a) Full compensation procedure for a sinusoidal physiological motion of 2 Hz b) Displacement of the corresponding last 5 periods from which the motion error, i.e. the final resultant motion (black line), was calculated.

TABLE I

RESULTS, OVER 5 GROUPS OF EXPERIMENTS PER FREQUENCY.

Frequency (Hz)	Motion (μm)						Compensation Percentage (%)	
	RMSE		MAE		NRMSE			
	Mean	STD	Mean	STD	Mean	STD	Mean	STD
1	2.15	0.44	4.37	1.01	7.17	1.55	85.45	3.57
2	2.64	0.63	5.34	1.21	8.95	2.11	81.86	4.04
3	3.03	0.42	7.20	0.51	10.13	1.40	75.91	1.84

means and standard deviations (STD) at each frequency is shown in Table I. The first metric was the root mean square error (RMSE):

$$\text{RMSE} = \sqrt{\frac{\sum_i^N (x_i - \hat{x}_i)^2}{N}}, i = 0, 1, 2, ..., N, \quad (2)$$

where x and $\hat{x}$ represent respectively the physiological motion and the pipette motion measured by the laser. N is the total number of data points within the five periods of motion, i.e. $N = 5 \cdot T \cdot f_d$, where T is the time in seconds for one period of physiological motion and f_d is the frequency in Hertz at which the motion data points are stored. Hence, in this case, $N = 5 \cdot 0.5 \cdot 25 = 62.5 \approx 63$ data points. Therefore, x_i corresponds to the absolute distance of the pipette at the time $\frac{i}{f_d}$. The second metric was the maximum absolute error (MAE):

$$\text{MAE} = \max\left\{|\hat{x}_i - x_i|\right\}, i = 0, 1, 2, ..., N. \quad (3)$$

The third metric was the normalized root mean square error (NRMSE) [28]:

$$\text{NRMSE} = \frac{\text{RMSE}}{x_{\max} - x_{\min}}. \quad (4)$$

The last metric was the compensated percentage (CP) and was calculated as follows:

$$\text{CP} = \left(1 - \frac{\text{MAE}}{x_{\max} - x_{\min}}\right) \times 100. \quad (5)$$

The set amplitude and hence range of the physiological motion was 31 μm, but the exact value used in this calculation was derived from the laser measurements for each experiment with a mean of 34.1 μm.

D. Results: Reaction Speed

The aim of the second experiment was to analyze the responsiveness of the compensation algorithm to a change in motion frequency. In the example in Fig. 7, the frequency of 2 Hz was increased by 3 steps of 0.1 Hz. The reaction time taken for the motion compensation for each step was about 12, 14, and 20 seconds respectively. It was found that this reaction time highly depends on the size of the frequency step, whether the frequency is an integer value and the size of the FFT window. A larger frequency step and a smaller FFT window lead to a faster reaction time. The FFT also measures the integer frequencies more accurately and hence the compensation occurs much faster and remains more stable. The average reaction time range varied between 4 and 30 seconds.

V. DISCUSSION

Patch clamping is one of the various clinical techniques strongly impacted by physiological motion as the measuring pipette needs to approach and patch onto a moving neural membrane without puncturing it. Motion compensation techniques in literature heavily rely on imaging technology or animal ECG measurements to cope with the lack of visibility of neurons [10], [11], [12], [13]. This can make the setup more complex and increase the costs of the experiments.

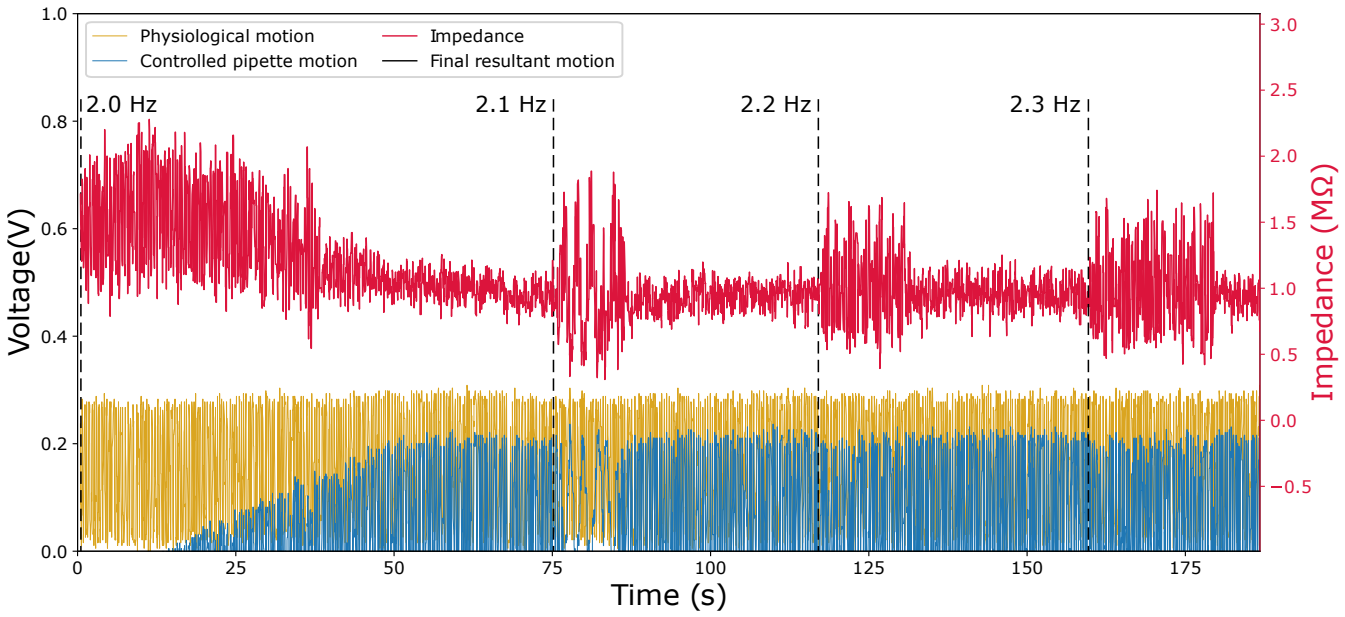


Fig. 7. Motion re-compensation based on EBI measurements when changing the frequency of the physiological motion from 2 Hz to 2.3 Hz in steps of 0.1 Hz during compensation.

Compared to this complicated approach, this paper presents a proof of concept of a motion compensation algorithm that solely relies on bio-impedance measurements to measure and characterize the relative physiological motion between the pipette tip and the neuron membrane. The algorithm uses a model-based method to characterize and compensate for the sinusoidal relative motion as there is no exact impedance-distance available.

The experimental validation showed that the program successfully compensates this physiological motion by $(85.5 \pm 3.6)\%$ at 1 Hz, $(81.86 \pm 4.04)\%$ at 2 Hz, and $(75.9 \pm 1.8)\%$ at 3 Hz. Note that as the heart rate increases, the CP gradually decreases. One of the reasons for this is the rate-dependent hysteresis of the piezoelectric actuator. However, in this work, we are targeting motion compensation induced by heartbeat, which is rarely over 3 Hz [29]. Thus, the influence of hysteresis from the actuator is very limited and is not considered in this work. The performance of the proposed algorithm could be improved slightly by compensating for the hysteresis. To address this problem, the analytical model methods [30] and deep learning methods [31] could be considered as future work for hysteresis compensation.

The first experiment further showed that motion compensation was maintained until the program was manually stopped, indicating the robustness of the algorithm when there is no change in physiological motion. The second experiment proved that the algorithm was able to automatically react to a change in frequency and re-compensate the motion as expected. This shows that even with an unstable heart rate, this algorithm could compensate for the physiologically induced motion. However, there was still a large variability in the reaction time, which would affect the responsiveness of the algorithm during the patch clamping procedure. The delayed response would have a greater effect on high-frequency motion, which could further explain why the CP decreases with increasing heart rate. Future work could focus on further quantifying the effect of the FFT window and the frequency step size on the reaction time to optimally fine-tune the algorithm parameters. However, the patch clamping experiments are often performed as long as the animals are alive [32]. Hence, the current responsiveness is already acceptable within this long time frame.

Both the relatively high CP and the ability to adapt to changes in physiological motion validate the use of this motion-compensation algorithm for patch clamping. The impedance-distance characterization presented in this paper could also signal close approach and provide markers to trigger motion compensation. Therefore, the use of EBI provides new potential for the development of a fully automated patch clamping robot compared to the image-guided approach [13].

VI. CONCLUSIONS

This paper proposes a new model-based motion compensation algorithm for patch-clamping, based solely on EBI measurements. The algorithm characterizes the sinusoidal physiological motion and replicates this motion in order to obtain zero net movement between the pipette tip and the neuron membrane in order to prevent puncturing the neurons. Future work should focus on reducing the reaction speed of the program during compensation and expanding the model such that sinusoidal motion with multiple frequencies can also be characterized. This proof of concept yielded promising results and its further development could lead to a significant contribution to a fully automated patch clamping robot.

REFERENCES

[1] C. Bargmann *et al.*, "Brain 2025: a scientific vision," *Brain Research through Advancing Innovative Neurotechnologies (BRAIN) Working Group Report to the Advisory Committee to the Director, NIH*, 2014.

[2] E. Verschooten *et al.*, "Auditory nerve frequency tuning measured with forward-masked compound action potentials," *J. of the Assoc. for Res. in Otolaryngology*, vol. 13, no. 6, pp. 799–817, 2012.

[3] W. M. Carroll, "The global burden of neurological disorders," *The Lancet Neurology*, vol. 18, no. 5, pp. 418–419, 2019.

[4] E. Verschooten, L. Robles, D. Kovačić, and P. X. Joris, "Auditory nerve frequency tuning measured with forward-masked compound action potentials," *Journal of the Association for Research in Otolaryngology*, vol. 13, no. 6, pp. 799–817, 2012.

[5] B. G. Kornreich, "The patch clamp technique: principles and technical considerations," *Journal of Veterinary Cardiology*, vol. 9, no. 1, pp. 25–37, 2007.

[6] C. Tao, G. Zhang, Y. Xiong, and Y. Zhou, "Functional dissection of synaptic circuits: in vivo patch-clamp recording in neuroscience," *Frontiers in neural circuits*, vol. 9, p. 23, 2015.

[7] J. Muthuswamy, M. Okandan, T. Jain, and A. Gilletti, "Electrostatic microactuators for precise positioning of neural microelectrodes," *IEEE Transactions on Biomedical Engineering*, vol. 52, no. 10, pp. 1748–1755, 2005.

[8] N. L. Anderson, "Pet rodents," *Saunders Manual of Small Animal Practice*, p. 1881, 2006.

[9] P. Flecknell, "Anaesthesia of animals for biomedical research," *BJA: British Journal of Anaesthesia*, vol. 71, no. 6, pp. 885–894, 1993.

[10] M. S. Fee, "Active stabilization of electrodes for intracellular recording in awake behaving animals," *Neuron*, vol. 27, no. 3, pp. 461–468, 2000.

[11] W. M. Stoy, B. Yang, A. Kight, N. C. Wright, P. Y. Borden, G. B. Stanley, and C. R. Forest, "Compensation of physiological motion enables high-yield whole-cell recording in vivo," *Journal of neuroscience methods*, vol. 348, p. 109008, 2021.

[12] S. Lee, Y. Nakamura, K. Yamane, T. Toujo, S. Takahashi, Y. Tanikawa, and H. Takahashi, "Image stabilization for in vivo microscopy by high-speed visual feedback control," *IEEE Transactions on Robotics*, vol. 24, no. 1, pp. 45–54, 2008.

[13] H.-J. Suk, E. S. Boyden, I. Van Welie, B. D. Allen, S. B. Kodandaramaiah, and C. R. Forest, "Image-guided closed-loop robotic system for automated whole-cell patch clamping electrophysiology of neurons in vivo," May 4 2021, uS Patent 10,993,634.

[14] S. B. Kodandaramaiah, G. L. Holst, I. R. Wickersham, A. C. Singer, G. T. Franzesi, M. L. McKinnon, C. R. Forest, and E. S. Boyden, "Assembly and operation of the autopatcher for automated intracellular neural recording in vivo," *Nature protocols*, vol. 11, no. 4, pp. 634–654, 2016.

[15] L. Cheng and M. Tavakoli, "Ultrasound image guidance and robot impedance control for beating-heart surgery," *Control Engineering Practice*, vol. 81, pp. 9–17, 2018.

[16] M. J. Musa, K. Sharma, K. Cleary, and Y. Chen, "Respiratory compensated robot for liver cancer treatment: Design, fabrication, and benchtop characterization," *IEEE/ASME Transactions on Mechatronics*, vol. 27, 2022.

[17] G. Li *et al.*, "A fully actuated body-mounted robotic assistant for MRI-guided low back pain injection," in *2020 IEEE International Conference on Robotics and Automation (ICRA)*. IEEE, 2020, pp. 5495–5501.

[18] Z. Jiang, N. Danis, Y. Bi, M. Zhou, M. Kroenke, T. Wendler, and N. Navab, "Precise repositioning of robotic ultrasound: Improving registration-based motion compensation using ultrasound confidence optimization," *IEEE Transactions on Instrumentation and Measurement*, vol. 71, pp. 1–11, 2022.

[19] Z. Cheng, A. S. Zeltner, A. T. Årsvold, K. L. Schwaner, P. T. Jensen, and T. R. Savarimuthu, "Active search of subsurface lymph nodes using robot-assisted electrical impedance scanning," *IEEE Transactions on Instrumentation and Measurement*, vol. 71, pp. 1–11, 2022.

[20] L. Schoevaerdts, L. Esteveny, A. Gijbels, J. Smits, D. Reynaerts, and E. Vander Poorten, "Design and evaluation of a new bioelectrical impedance sensor for micro-surgery: application to retinal vein cannulation," *International journal of computer assisted radiology and surgery*, vol. 14, no. 2, pp. 311–320, 2019.

[21] L. Schoevaerdts, G. Borghesan, M. Ourak, D. Reynaerts, and E. Vander Poorten, "Electrical bio-impedance proximity sensing for vitreoretinal micro-surgery," *IEEE Robotics and Automation Letters*, vol. 4, no. 4, pp. 4086–4093, 2019.

[22] Z. Cheng, K. L. Schwaner, D. Dall'Alba, P. Fiorini, and T. R. Savarimuthu, "An electrical bioimpedance scanning system for subsurface tissue detection in robot assisted minimally invasive surgery," *IEEE Transactions on Biomedical Engineering*, vol. 69, 2022.

[23] P. B. Ishai, M. S. Talary, A. Caduff, E. Levy, and Y. Feldman, "Electrode polarization in dielectric measurements: a review," *Measurement science and technology*, vol. 24, no. 10, p. 102001, 2013.

[24] P. M. Loschak, A. Degirmenci, C. M. Tschabrunn, E. Anter, and R. D. Howe, "Automatically steering cardiac catheters in vivo with respiratory motion compensation," *The International journal of robotics research*, vol. 39, no. 5, pp. 586–597, 2020.

[25] N. A. Wood, D. M. Del Agua, M. A. Zenati, and C. N. Riviere, "Position estimation of an epicardial crawling robot on the beating heart by modeling of physiological motion," in *2011 IEEE/RSJ International Conference on Intelligent Robots and Systems*. IEEE, 2011, pp. 4522–4527.

[26] M. Faulkner, S. Hannan, K. Aristovich, J. Avery, and D. Holder, "Characterising the frequency response of impedance changes during evoked physiological activity in the rat brain," *Physiological measurement*, vol. 39, no. 3, p. 034007, 2018.

[27] Y. Zhang *et al.*, "Controlling of a micropositioning piezoelectric actuator using an lstm network for robotic eye surgery," in *Conference on New Technologies for Computer and Robot Assisted Surgery, Location: Napoli*, 2022.

[28] D. Wu *et al.*, "Hysteresis modeling of robotic catheters based on long short-term memory network for improved environment reconstruction," *IEEE Robotics and Automation Letters*, vol. 6, no. 2, pp. 2106–2113, 2021.

[29] P. Flecknell, "Anaesthesia of animals for biomedical research," *BJA: British Journal of Anaesthesia*, vol. 71, no. 6, pp. 885–894, 1993.

[30] S. Shakiba *et al.*, "Modeling and compensation of asymmetric rate-dependent hysteresis of a miniature pneumatic artificial muscle-based catheter," *Mechanical Systems and Signal Processing*, vol. 154, p. 107532, 2021.

[31] D. Wu *et al.*, "Deep-learning-based compliant motion control of a pneumatically-driven robotic catheter," *IEEE Robotics and Automation Letters*, vol. 7, no. 4, pp. 8853–8860, 2022.

[32] M. Kang *et al.*, "A review of the ethical use of animals in functional experimental research in china based on the "Four R" principles of reduction, replacement, refinement, and responsibility," *Medical Science Monitor*, vol. 28, 2022.